International Journal of Mass Spectrometry 275 (2008) 64–74

Contents lists available at ScienceDirect

International Journal of Mass Spectrometry

journal homepage: www.elsevier.com/locate/ijms

An extraction system for low-energy hydrogen ions formed by electron impact

Sabina Markelj*, Zdravko Rupnik, Iztok Čadež

Jožef Stefan Institute, Jamova cesta 39, 1000 Ljubljana, Slovenia

ARTICLE INFO

Article history:
Received 21 March 2008
Received in revised form 9 May 2008
Accepted 15 May 2008
Available online 24 May 2008

Keywords:
Hydrogen ion
Ion optics
Dissociative electron attachment
Vibrational spectrometry

ABSTRACT

A system has been developed for extracting near-zero kinetic energy H^- and D^- ions formed by dissociative electron attachment. It is the essential part of a new set-up for vibrational spectroscopy of hydrogen molecules. A magnetic field is used to collimate the probing electron beam. Ions produced by electron collision with the target molecules are collected by the combined action of this field and an electrostatic field penetrating into the interaction region. Highly effective extraction is achieved by taking into account the correct out-of plane displacement of ion trajectories which is usually neglected in similar arrangements. The extraction conditions are mass dependent so that by proper tuning, mass selection of detected ions is achieved. The new system is also used for detecting positive ions created by electron collisions with hydrogen atoms and molecules.

1. Introduction

Experimental systems with a magnetically confined electron beam are used quite often in those mass spectrometry experiments where ionization and dissociative attachment are studied (e.g. [1–4]). Such systems take advantage of the fact that the magnetic field required to collimate a low-energy electron beam is rather small, typically around 10 mT, and that such a field does not significantly perturb the trajectories of much heavier ions that are produced by electron impact in the interaction region. While this is a reasonable assumption for heavy and fast ions it is not so for slow and light ones, especially not for hydrogen. Detection of hydrogen ions is performed in various diagnostic techniques, so that achieving high detection effectiveness and reliable determination of hydrogen ion production yield is important for an effective and accurate quantitative analysis.

Vibrational spectroscopy of hydrogen molecules based on properties of dissociative electron attachment (DEA), $e + H_2 \rightarrow H_2^- \rightarrow H^- + H$, is one of the diagnostic techniques requiring effective detection of low energy hydrogen ions. By this method [5–7], the yield of near-zero kinetic energy H^- ions is measured as a function of electron energy in the energy range between 0 and 5 eV. The contribution of different vibrational states in such spectra can be identified due to the properties of DEA in hydrogen. Namely, the threshold for the excited molecule is lower by the excitation energy, than for the ground state and the cross section is peaked at the respective threshold. Additionally, the peak cross section increases strongly with vibrational excitation of the target molecule. The population of vibrational states in the target gas is deduced from the measured ion yield spectra by an appropriate deconvolution technique. This method is applicable to different hydrogen isotopologues (H_2, HD, D_2), since the properties of DEA are the same, so that either H^- or D^- has to be detected. The drawback of the method is the lower energy resolution than that of available optical methods, so that individual rotational contributions cannot be resolved. However, an important advantage of the method is its relative simplicity and very high sensitivity for excited molecules because the DEA cross section reaches the gas kinetic cross sections (in the 10^{-15} cm^2 range) for the highest states of all isotopologues.

We have constructed a new set-up for hydrogen vibrational spectroscopy that is based on the above principle [8,9]. The new instrument is intended to enable a systematic study of processes involving vibrationally excited hydrogen molecules that are important for fusion edge plasmas. Neutral atoms and molecules are created by ion recombination on the wall of the fusion reactor and on the other plasma facing components. They play an important role in reducing power load to the walls and in surface processes such as chemical erosion of carbon deposits. Neutral molecules are especially important for ion recombination and plasma detachment in tokamak divertors, since they take part in various atomic collision processes in the edge plasma.

Here we describe the principle of operation, construction details and performance of the system for extracting and detecting of low-energy hydrogen ions used in the new apparatus. The system has to fulfill two main goals: (i) high ion detection effectiveness peaking

* Corresponding author.
E-mail address: sabina.markelj@ijs.si (S. Markelj).

1387-3806/$ – see front matter © 2008 Elsevier B.V. All rights reserved.
doi:10.1016/j.ijms.2008.05.020

at very low energy, and (ii) separation of light ions of different mass (H^- or D^-). It also has to effectively reduce possible noise originating from stray electrons, metastable particles and UV photons. To ensure the above requirements for ion extraction we employ a penetrating electrostatic field immersed in a homogeneous magnetic field. The penetrating electrostatic field technique had been developed and employed successfully in purely electrostatic systems ($B=0$) for threshold electron impact ionization studies [10] and, since then, frequently used for almost 100% effective low-energy electron and ion collection (e.g. [5,11]). For the needs of the new experiment, that requires near-zero kinetic energy ion detection, we have modified the penetrating electrostatic field technique by the presence of a weak (5–10 mT) homogeneous magnetic field that is also used to collimate the electron beam. A preliminary description of this system has been given elsewhere [12]. Here, we describe the principle of operation of the new system accompanied by ion trajectory simulations, followed by construction details of the system and experimental tests of the extraction characteristics. Most of the results were obtained by measurements of H^- and D^- ions from the dissociative electron attachment. Finally, we also present some results obtained by detecting positive ions created by the electron impact ionization of atoms and molecules from an atomic hydrogen source.

2. Principle of operation and model analysis

The basic concept of the new spectrometer for hydrogen vibrational spectroscopy is shown schematically in Fig. 1. A probing electron beam from an electron gun is collimated by a collinear magnetic field B. The electron beam crosses the interaction region (IR) into which the test target gas is introduced, and then dumped in the Faraday cup collector. Negative ions formed in the IR by DEA are extracted by a weak electric field created by a set of plate electrodes parallel to the e-beam. Following extraction and mass and energy filtering, the ions are detected by a channel electron multiplier. Such a spectrometer configuration was chosen in order to have simple control of the required low-energy (0.1–5 eV) electron beam. The ion extraction system is based on the original concept of a penetrating electrostatic field in the presence of a homogeneous magnetic field. This configuration also enables mass separation of light ions of interest (H^- and D^-) and prevents stray electrons and heavier ions from background from reaching the channel electron multiplier.

The electrostatic penetrating field ensures high collection effectiveness for very low ("near-zero") kinetic energy ions and, at the same time, low transmission probability for the high energy ones. In this way, sharp peaks in the ion yield spectrum are obtained at the DEA thresholds in the case of vertical onset, which is the case for hydrogen. Namely, two DEA channels in H_2 exhibit a vertical threshold, i.e. the cross section is finite and, in these cases, it has even its highest value just above the threshold where the dissociative channel of resonant state stabilisation opens. This is the case for the process having thresholds at 3.72 eV ("4 eV" process in the following text) and at 13.92 eV ("14 eV" process). Because all incident electron energy is transferred to the two fragments of dissociation, the energy of the created ion is:

$$E_i = \frac{M_a}{M_m}(E_e - E_{Th}), \quad (1)$$

where M_a is the mass of the neutral atomic fragment, M_m is the mass of the molecule, E_e is the incident electron energy and E_{Th} the threshold energy. The threshold energy is determined from atomic and reaction parameters as $E_{Th} = D_0 + E_{Exf} - EA - E_{Exi}$, D_0 being the dissociation energy of the ground state molecule, EA the electron affinity of the ionic fragment and E_{Exf} and E_{Exi} the internal excitation energies of the fragments of dissociation and target molecule respectively. M_a/M_m is equal to 1/2 in both the cases presently studied, i.e. H^-/H_2 and D^-/D_2, but is 2/3 and 1/3 for the also relevant cases of H^-/HD and D^-/HD.

To create the penetrating field needed for the preferential detection of near-zero kinetic energy ions we chose electrodes with a rectangular aperture. Due to the strong astigmatic characteristics (e.g. [13]) of a lens composed of such electrodes, the resulting electrostatic field is well suited for the present application. Namely, we need to extract ions from the elongated cylindrical interaction region formed by a parallel e-beam traversing a broad target gas.

A detailed simulation of ion rays in a model system was undertaken before deciding on the shape and configuration of the electrodes. Ion trajectories were computer simulated by the charged particle optics program CPO3D (http://www.electronoptics.com/). After an extensive study of different positions of individual electrodes and different sizes of rectangular apertures, the chosen electrode system is shown in Fig. 2. The *X*-axis of the coordinate system is defined by the electron beam (collinear with B), the *Y*-axis is perpendicular to the extraction electrodes (general direction of extraction) and the *Z*-axis is perpendicular to two others. Two parallel electrodes, H2 and H3, that are kept at ground potential, limit the IR. The next electrodes, H4 and H5, create the penetrating

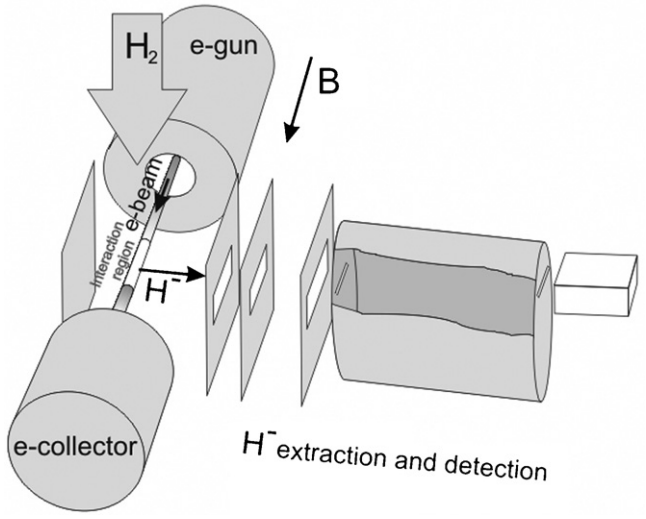

Fig. 1. Schematic representation of the set-up for hydrogen ro-vibrational diagnostics based on the dissociative electron attachment.

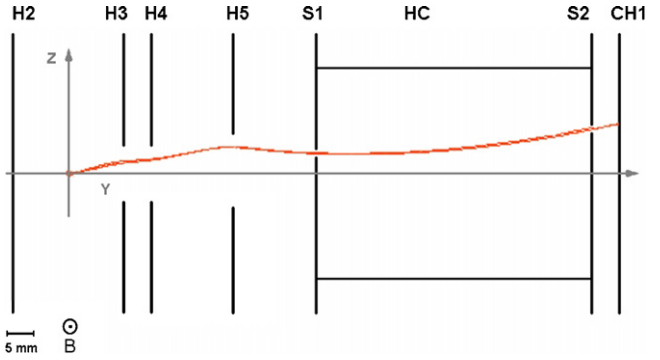

Fig. 2. Extraction electrode system used for the CPO3D simulation. One calculated trajectory of an H^- ion having 2 meV initial energy and starting at the centre of IR is shown. Potentials on electrodes H2, H3, H4, H5, HC and CH1 are 0, 0, 20, 20, 250, 250 V respectively. The trajectory is calculated with a 10 mT magnetic field.

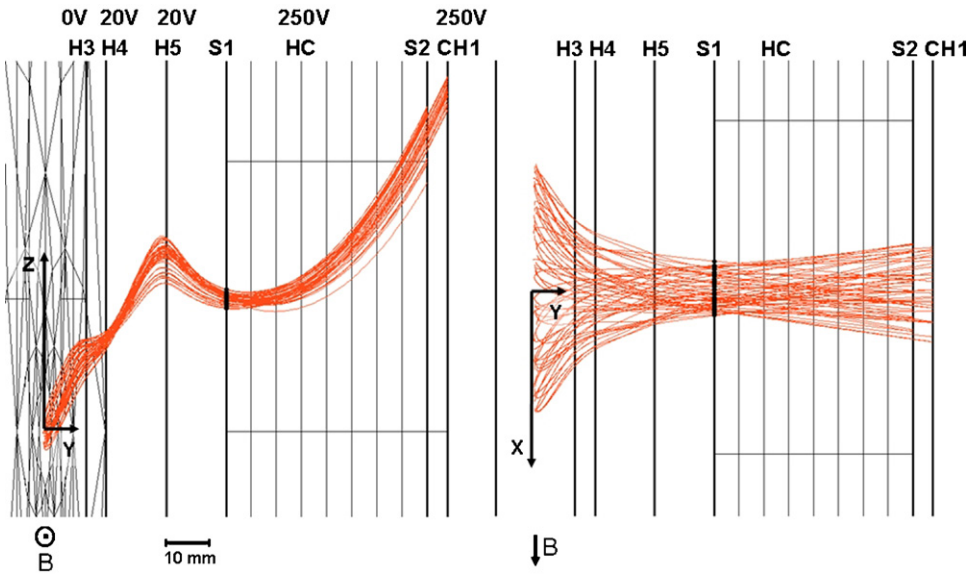

Fig. 3. Projections of 2 meV H^- rays calculated by CPO3D in *ZY* (a) and *XY* (b) planes. For clearer presentation of the perpendicular motion of ions, the *Y*-axis is compressed by a factor of five relative to the *X* and *Z*-axes. Potentials on electrodes and the magnetic field are the same as in Fig. 2.

extraction field through the rectangular aperture in the electrode H3. A cylindrical electrode HC, coaxial with the *Y*-axis, is maintained at the higher potential needed for proper ion focusing on the slit S1 mounted on the entrance side of HC. Ions travel between the entrance slit S1 and exit slit S2 through a space free of electric field, and encounter the ion detector after passing S2. The electrode HC with slits S1 and S2 is the main filter for particles on their way from IR to the ion detector.

Wide rectangular apertures were used in the extraction electrodes to accommodate the linear interaction region geometry along the e-beam. The sizes of the rectangular slits in the electrodes are 10 mm × 20 mm for H3, 10 mm × 12 mm for H4, and 12 mm × 20 mm for H5—the first dimension is in the *Z* and the second in the *X* direction. The slits S1 (1 mm × 20 mm) and S2 (1 mm × 15 mm) are parallel to the *X*-axis and are positioned out of the *XY* plane at respective heights $h_1 = 3.5$ mm and $h_2 = 8$ mm in the *Z* direction. *Y*-coordinates of electrodes H2 to H5 and slits S1 and S2 are −10, 10, 15, 30, 45 and 95 mm.

The magnetic field of two appropriate current loops, simulating real Helmholtz coils, is used in the model ray tracing. For the simulation we restricted the extraction conditions such that applied voltages on H4 and H5 were kept at the same value, and the central magnetic field at $B = 10$ mT. Optimal focusing conditions at the S1 slit in both planes *YZ* and *XY*, with high transmission for low energy ions, were determined by varying the applied voltages on the electrodes. The principle of achieved ion extraction is illustrated by the bunch of calculated trajectories of H^- shown in Fig. 3. Applied voltages on the electrodes H2, H3, H4, H5, HC and CH1 are 0, 0, 20, 20, 250, 250 V respectively and initial ion energy is 2 meV. The projection of the trajectories in the *YZ* plane is shown in Fig. 3a while the projection in the *XY* plane is presented in Fig. 3b. The scale is compressed by a factor of 5 in the direction of the *Y*-axis to show better the ion motion in the *Z* direction. Low energy ions starting at the *X*-axis are accelerated in the *Y*-direction by the penetrating field being slightly convergent in the *XY* and *ZY* planes. By the combined action of both the electric and magnetic fields, the bunch of trajectories deviate from the *Y*-axis in the *Z*-direction and are most compressed close to the H4 electrode. After passing H5, they are bent back towards the *Y*-axis and their trajectories are then roughly parallelized though still compressed. If correct voltages are applied the ions pass the limiting slit S1 and enter the space between S1 and S2 where no electric field is present. Only ions having adequate initial velocities at S1 will traverse exit slit S2 and will subsequently be detected by the channel electron multiplier. In this way the slit S2 acts as a filter for the velocity of ions in the plane of S1. The pair of slits S1 and S2 acts as a rough mass filter. Trajectories of ions in the *XY* plane are characterized mainly by the converging action of rectangular apertures in electrodes H3 to H5. In this way ions from an extended part of IR are collected and transferred to the ion detector.

Ion extraction characteristics obtained by model analysis are illustrated in Figs. 4 and 5. Electric and magnetic fields are the same as for the trajectories in Figs. 2 and 3. In Fig. 4, the *Z*-displacement at the plane of the slit S1 is shown for H^- and D^- ions having different initial energies. For each ion's energy twenty trajectories were calculated with a random starting point within a cylinder 26 mm long and 1 mm in diameter, placed symmetrically along the *X*-axis. Initial directions of ion velocity were also randomly distributed. The

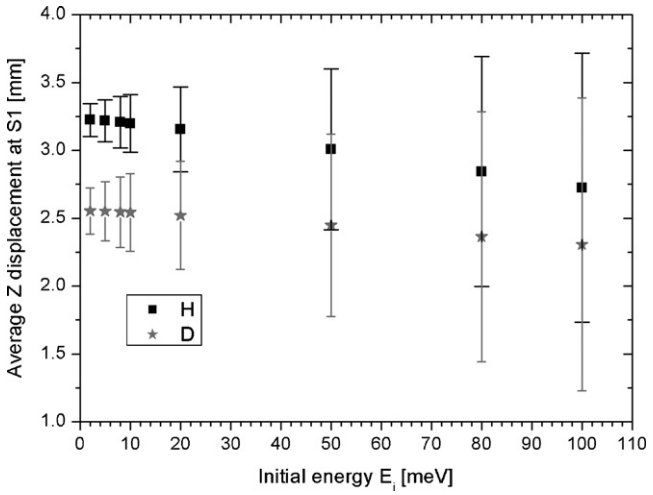

Fig. 4. Mean value and standard deviation of the displacement in the *Z* direction at the S1 plane of H^- and D^- trajectories for different initial ion energies. This characteristic is the basis for mass selectivity of the present extraction system.

mean displacement and its standard deviation at the plane of S1 are shown as a function of the energy of the ions. The focusing points for H^- and D^- ions are different under the same extraction conditions. There is good focusing of ions having energies below about 10 meV: ions starting from the 1 mm diameter cylinder are focused on a 0.5 mm wide image in the plane of S1. For higher energy ions the spread in the S1 plane becomes larger and mixing of H^- and D^- occurs at the same place. Preferential transmission of low energy ions and particular ion mass is achieved by proper placing of the slit in this plane. By varying the extraction voltages and/or magnetic field the distribution of ions at the S1 plane moves across the slit, facilitating tuning of the selection of desired ions.

The high effectiveness of preferential detection of low kinetic energy ions as described above is illustrated in Fig. 5. The transmission effectiveness for H^- is shown for the case where a 1 mm slit placed at height h_1 = 3.5 mm is used for S1. The transmission effectiveness is defined as the ratio of the number of ions transmitted through the slit to the total number of ions of a particular set, starting randomly from the interaction region. It is shown as a function of the initial ion energy in Fig. 5 for two lengths of starting regions, 10 and 26 mm. The ion transmission characteristic peaks at zero energy and, for this geometry, decreases to 50% for energy of about 0.1 eV. The length of HC and the position and the size of the S2 slit were determined by analysis of ion trajectories in the region of HC after S1.

The crucial element for ion mass and energy selection is the slit S1 in the HC electrode, where ions from the interaction region form a narrow line image. The second slit S2 is used for better separation of H^- from D^- ions. Some D^- ions may still come through the first slit when the conditions are optimal for H^-, but the trajectory radius in the homogeneous magnetic field is different for ions with different masses and the same energy, so they cannot cross S2 and reach the ion detector.

An inherent characteristic of penetrating field techniques is that the electrostatic field is present in the interaction region and, to some extent, perturbs both the incident electron beam and the starting conditions for created ions. While, in a purely electrostatic case, the penetrating field can be very weak, this is not so when the magnetic field is present. In this case, the field must be stronger so that ion trajectories can be sufficiently stratified to reach the region of higher potential, from H5 on in the present case.

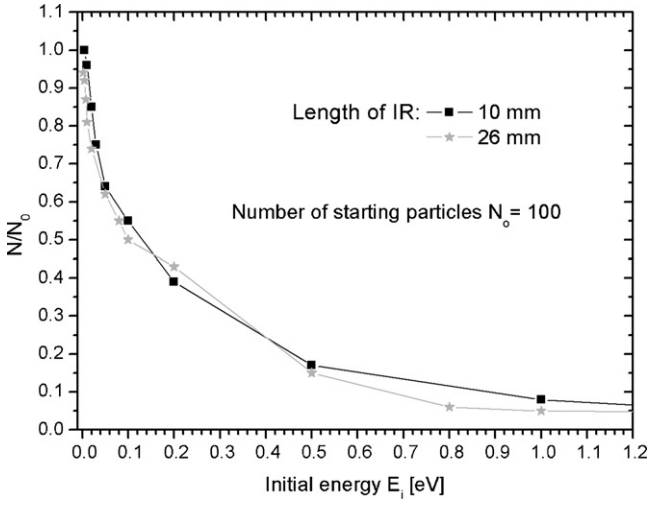

Fig. 5. The H^- transmission effectiveness as a function of initial ion energy as determined from CPO3D simulation of the electrode system from Fig. 2. The entrance slit S1 (1 mm × 10 mm) was placed at the entrance of HC.

Three applications can be envisaged for the extraction system described in this paper. The first is of primary importance here, i.e. the detection of negative ions from DEA. The penetrating field influences both the e-beam and the starting conditions of the created ions, producing an energy dependent e-beam displacement in IR and also broadening of the energy distribution of electrons. Due to the latter effect, the ions created by DEA at different positions in the IR have slightly different energies, according to Eq. (1). To keep trajectory simulations by CPO reasonably simple we neglected the influence of the penetrating field on the e-beam in the present treatment.

In the application, in which positive ions are extracted and detected, the influence of the penetrating field on the e-beam position is less pronounced due to the higher electron energy needed for ionization (above 10 eV). Also, the energy of parent ions created by the electron impact depends only weakly on the incident energy. However, the variation of electron energy in IR, produced by the penetrating field, provokes the variation of the ion production rate due to energy dependence of the ionization cross section. This effect is the most pronounced in the threshold region.

The potential application of the present extraction system is the collection of ions from photoionization. In this case the penetration potential in IR would only cause different final energy of ions created at different locations in IR.

3. Experimental set-up

Two perpendicular cuts through the electrode system of the spectrometer are shown in Fig. 6. As before, the coordinate system is defined by the electron beam (*X*-axis), the general direction of ion extraction (*Y*-axis) and the direction of the sample gas inlet (*Z*-axis). The extraction and detection system consist of flat disk electrodes H1 to H5, a cylindrical electrode HC and a channel electron multiplier. H1 is a disk electrode with no aperture, that serves as an auxiliary total ion current collector. The entrance of the channel electron multiplier (size 5 mm × 15 mm) is denoted by CH1 and its anode by CH2. Two slits, S1 and S2, parallel to the *X*-axis at their respective heights h_1 and h_2 (along the *Z*-direction) are mounted at the entrance and exit base of HC. All electrodes are made of titanium and the support elements of an aluminium alloy.

A simple, low-resolution electron gun with a 0.8 mm tantalum disc cathode was employed to produce the electron beam for the present tests of the extraction optics. The cathode was kept at low temperature (about 2000 K) in order to avoid the space charge effects. Electrons are dumped in the electron collector after passing the interaction region. Due to the simple construction of the electron gun we can use the standard energy distribution function for the thermionic electron emission (e.g. [14]):

$$\frac{dP}{dE} = \frac{E}{(kT_C)^2} e^{-E/kT_C}, \quad (2)$$

where T_C is the cathode temperature and k the Boltzmann constant. The shape of the electron beam current versus electron energy at E = 0 eV confirms our assumption that the energy distribution of the incident electron beam is well represented by (2). The electron beam current was typically in the 100 nA range and the energy spread was 0.3–0.5 eV. A pair of Helmholtz coils produced a magnetic field coaxial with the electron beam and the most of the present tests were performed with a field strength between 5 and 7 mT.

The dimensions of apertures, slits and positions of individual electrodes are as quoted in the previous section when describing the model analysis. The only difference is that the electrode H2 has a rectangular aperture of the same size as H3 (10 mm × 20 mm). Some

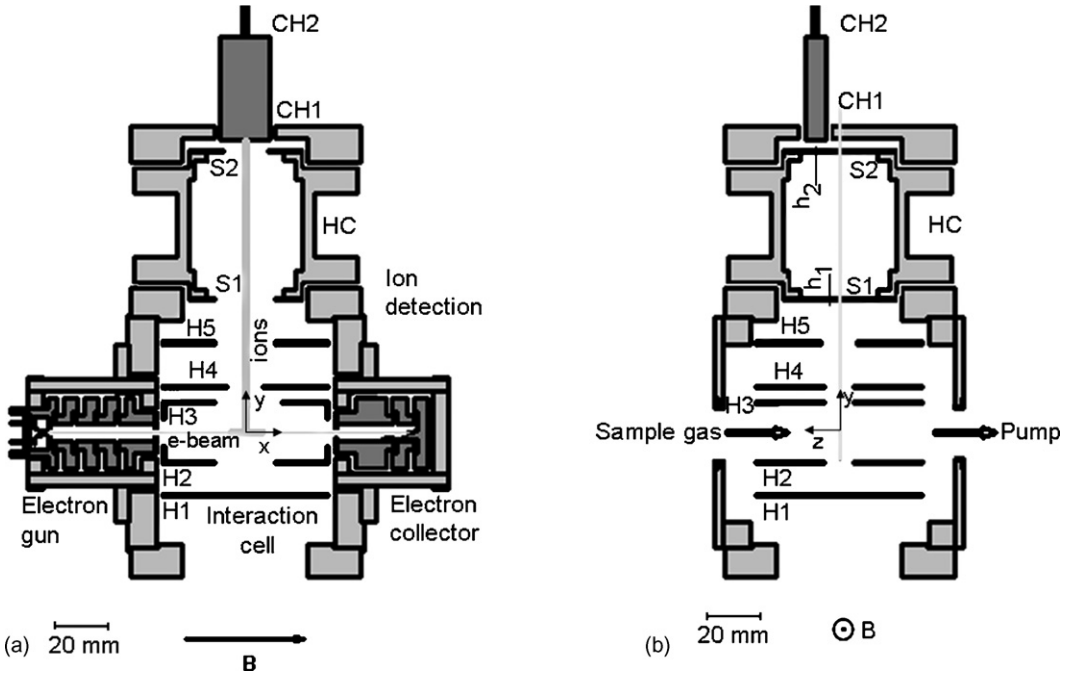

Fig. 6. Schematic drawing of the system. (a) *XY* cut and (b) *ZY* cut of the ion extraction and detection system of the spectrometer.

different sizes of the slit S1 were tested and results are discussed in the next section.

The test gas is introduced through the top of the mounting block for the electrode system as shown in Fig. 6b, and can be considered evenly distributed within IR for the purpose of present extraction study.

The operation of the experiment is PC controlled by a set of programs written in LabVIEW, National Instrument's graphical development environment (http://www.ni.com). The main program runs the experiment in a multichannel scanning mode by simultaneous monitoring and/or controlling parameters of the experiment.

4. Results

The performance of the new ion extraction optics was studied by detecting low energy H^- and D^- ions created by DEA in H_2 and D_2. Attention is focused on the DEA processes that have the highest cross section at the threshold where reaction products (H^- and H for H_2 and D^- and D for D_2) are produced with zero kinetic energy. A typical low-energy H^- yield spectrum from H_2 obtained by energy variation of the electron beam between 0 and 19 eV is shown in Fig. 7. The 4 eV peak is due to the lowest energy DEA at which a ground state hydrogen atom is the neutral fragment. About twelve times higher, the 14 eV peak is also due to DEA but here, the hydrogen atom fragment is formed in the $n = 2$ electronically excited state. Besides these two main features of interest, a signal in the 6–10 eV region is also observed that is due to DEA in the water vapour from the vacuum background. Some smaller H^- signal is due to other DEA processes in hydrogen ($n > 2$) and also to non-resonant ion pair production ($e + H_2 \rightarrow H^- + H^+$) above its threshold at 17.3 eV. Finally, part of the detected signal is the background that originates from UV photons and metastable particles. This background is easily identified when the detection optics are tuned so that the charged particles are not transmitted, most easily by setting $U_{HC} = 0$ V. In the present study, we have focused on the 4 and the 14 eV DEA processes.

To illustrate the performance of the new ion extraction and detection system and to achieve optimal conditions for high ion transmission and good ion mass selectivity, we performed studies at different magnetic field strengths, different voltages applied to the electrodes, and different sizes of limiting slits.

4.1. High extraction voltage

Experimental checks were started under similar conditions that were deduced from CPO3D simulations in which electrodes H4 and H5 were kept at the same voltage. Optimal conditions were obtained with $U_{H4} = U_{H5} = 18$ V and magnetic field $B = 7.3$ mT. The effect of the U_{HC} on H^-/H_2 ion yield under these conditions is shown for the 4 eV peak in Fig. 8a and for the 14 eV peak in Fig. 8b. If U_{HC}

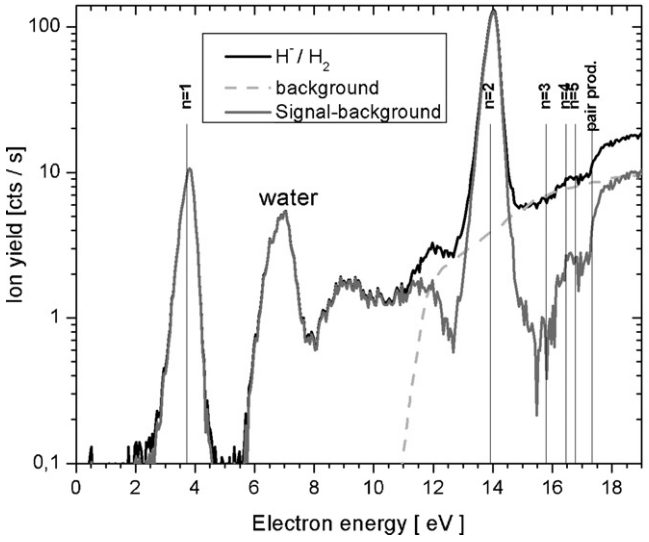

Fig. 7. A typical H^- yield spectrum from H_2 for the electron energy range 0–19 eV. The background that is due to UV photons and metastable neutrals is marked with a dashed line.

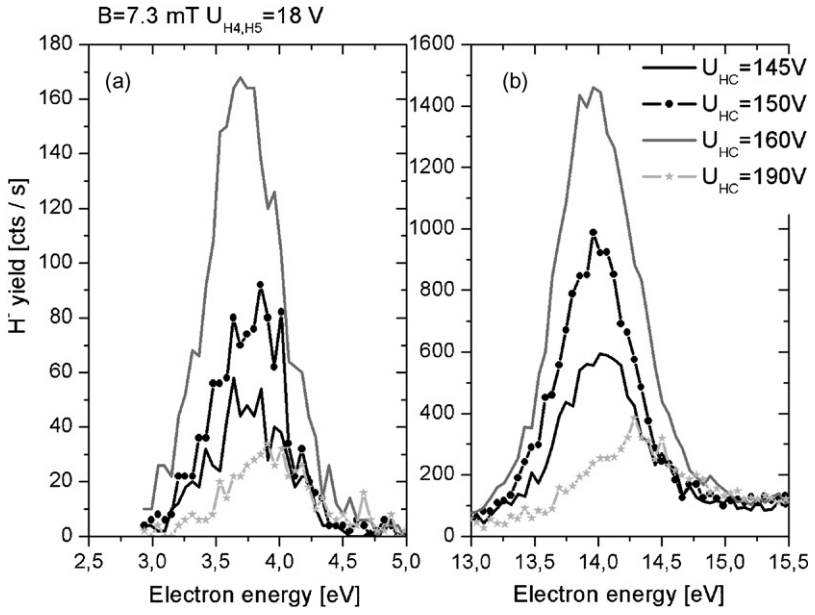

Fig. 8. Changing the 4 eV (a) and 14 eV (b) peaks for different U_{HC}. Extraction conditions as denoted in the figure.

is too low, the off-axis ion deflection produced by the magnetic field is not compensated by the alignment action of the accelerating electric field, so that ions hit the electrode HC above the slit S1. By increasing U_{HC} the Z displacement of the ion trajectories in the S1 plane decreases and, at a proper value of U_{HC}, ions pass the slit. The ions passing through S1 are created by DEA with a starting energy dependent on the electron energy $E_i = 1/2(E_e - E_{Th})$. Only the low energy ions are desired to be extracted and detected. Therefore, under optimal extraction conditions, the maximal signal near the threshold electron energy and thereafter a fast signal decrease at higher electron energies would be expected. However, if the extraction conditions (i.e. U_{HC}) are not adequate for the very low energy ions, the high-energy ions can still be extracted into the system and they contribute to the peak, as seen in Fig. 8. In this way, the dependence of peak shape on U_{HC} can be understood as referring to the results of ray tracing shown in Fig. 4. Very low energy ions are focused so that optimal transmission conditions regarding U_{HC} are within a relatively narrow range. On the other hand the higher energy ions are more spread in the bunch of trajectories of extracted ions and also contribute to the peak under non-ideal extraction conditions. As a consequence of this interplay between the electron and ion energies, and respective influence on the ion extraction effectiveness, the observed peak shape changes with U_{HC}. For this reason, a simple ion yield scan versus U_{HC} at constant electron energy at peak maximum does not give the true transmission function and mass selectivity of the extraction system. Therefore we performed a system analysis by recording the whole DEA peak for different conditions.

Ion trajectories calculated by the CPO3D program reproduced well the above-described optimal experimental condition. The calculation result for the set of H^- trajectories, starting with 5 meV initial energy from different intervals along X-axis is shown in Fig. 9. The conditions for extraction are 0, 0, 18, 18, 173 V for U_{H2} to U_{H5} and U_{HC}, and the magnetic field is 7.3 mT. A total of 100 ion trajectories were calculated. Ions started randomly from a cylinder 1 mm in diameter on the X-axis. The first 10 ions started from $x = 0$–2 mm, the next 10 ions from $x = 2$–4 mm, and so on. In Fig. 9a the mean Z displacement and its standard deviation in the plane of S1, $y = 44$ mm, is shown versus the initial X displacement. Ions that start at around $x = 0$ mm are displaced in the Z direction at $y = 44$ mm and focused at the slit S1. In Fig. 9b, the mean final X displacement and its standard deviation at the S1 electrode is shown for the same conditions and trajectories as for Fig. 9a. Strong compression of ion trajectories in the XY plane is illustrated. Calculation was performed also for other initial ion energies and they show similar characteristics only the standard deviation increases with the initial ion energy. Accordingly, effective focusing is achieved for the first 5 mm for energies bellow 10 meV. Focusing is also achieved in the XY plane, where ions with energy below 10 meV starting from around $x = 19$ mm are focused to 6 mm at $y = 44$ mm.

Mass selectivity for H^- and D^- was obtained experimentally by scanning the 14 eV DEA peak at different U_{HC} for the above conditions ($U_{H4} = U_{H5} = 18$ V, $B = 7.3$ mT). This analysis was made with the 14 eV peak because the cross section for DEA is much higher than for the 4 eV process. It is about twelve times higher in the case of

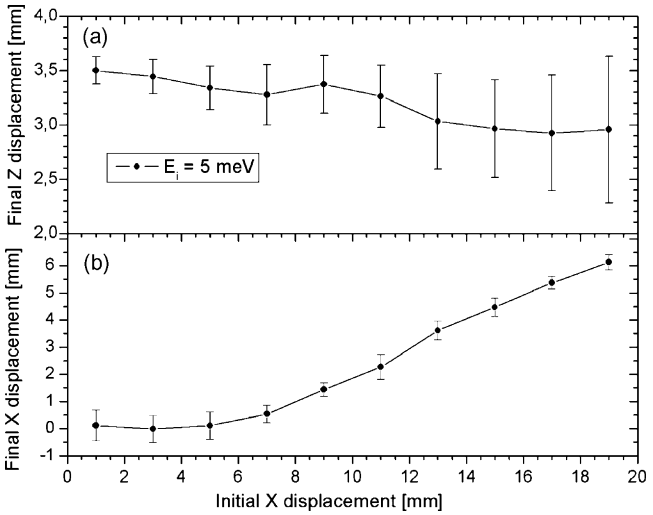

Fig. 9. (a) The mean displacement in the Z direction and its standard deviation before the slit S1 for 5 meV initial H^- ion energy as a function of the initial X displacement starting in IR at $y = 0$. (b) The mean displacement in the X direction and its standard deviation before the slit S1 for 5 meV initial H^- ion energy as a function of the initial X displacement. Extraction conditions are $B = 7.3$ mT $U_{H4} = U_{H5} = 18$ V and $U_{HC} = 173$ V.

H^-/H_2 and even more than a thousand times higher for D^-/D_2 [15] so that such a study would be impossible in deuterium. On the other hand, DEA properties of the 4 and 14 eV processes are very similar and some simultaneous check analyses made with both peaks in H_2 gave the same results.

The normalized 14 eV peak height dependence on U_{HC} for both isotopes, which best illustrates the mass selectivity, is shown in Fig. 10a. Data are obtained by dividing the measured ion yield peak height by its maximum value for each isotope. The H^- and D^- peaks overlap partially and, because of the asymmetric shape of the transmission functions, there is a greater contribution of D^- in the range of the best H^- condition than the converse. In order to increase the mass selectivity, the width of the slit S1 was reduced from 1 to 0.2 mm, marked as slit 1 and slit 2 respectively. The mass selectivity for both cases is shown in Figs. 10a and the results are summarized in Table 1. The same experimental data shown as a variation of relative peak height with U_{HC} are shown in Fig. 10b and summarized in Table 2. The relative peak height is defined as the maximum ion yield of the 14 eV peak in counts per second divided by the electron current and target gas pressure. The pressure of the target gas in IR was determined from the ion gauge reading by normalization to the absolute value with a capacitive manometer (IG reading multiplied by the experimentally determined K_d) and multiplied by the ratio of the ion yield when the gas is introduced directly in the interaction region to that through an auxiliary side port. In this way, the multiplying factor Sr is determined and represents the local density increase in IR with respect to the measured background pressure. The target gas pressure is therefore equal to $p\,[Pa] = Sr\,K_d\,p_{ind} = 1.47 \times 3.55 \times 1.333 \times 10^{-4} \times p_{ind}$, where p_{ind} is the pressure reading of the ion gauge in 10^{-6} Torr. By replacing the slit 1 with the slit 2, the maximum relative peak height, i.e. relative transmission of the system, decreased but the mass selectivity for the two isotopes improved. The relative transmission decreased by a factor of 2.4 for H^- and 2.9 for D^-, being less than the geometrical factor 5, indicating the degree of focusing in the plane of S1 slit.

On increasing voltages on H4 and H5 simultaneously, both the 4 and 14 eV peaks become broader, due to the increasing penetration field in the interaction region. Ions with higher energy are therefore drawn into the extraction system and detected more effectively. By increasing the penetration field, its influence on the incident electron beam also increases. Electrons are locally accelerated, as can be seen indirectly by displacement of the H^- peak towards lower electron energy.

4.2. Low extraction voltage

To decrease the influence of the penetrating field on the incident electron beam we analysed the performance of the system at lower U_{H4}. When decreasing U_{H4} from 18 V to 7 V the H^- yield decreased and the width of the peak narrowed. The potential in the centre of the interaction region decreased from 1 to 0.44 V. The potential of the H4 electrode contributes most to the penetrating field in IR, while the influence of U_{H5} and U_{HC} is rather weak. The latter two potentials can therefore be adjusted to optimal extraction with little concern for their influence in the IR.

For further analysis of the system, U_{H4} was set constant to 7 V and the magnetic field strength B and potentials U_{H5} and U_{HC} were varied. Checks were also performed for different sizes and positions of S1 denoted as follows: slit 1: 1 mm × 20 mm at h_1 = 3.5 mm, slit 2: 0.2 mm × 20 mm at h_1 = 3.5 mm, slit 3: 1 mm × 10 mm at h_1 = 3.5 mm and slit 4: 1 mm × 10 mm at h_1 = 3.8 mm. In Fig. 11 the 14 eV peak shape (Fig. 11a) and relative transmission intensity for the 14 eV peak (Fig. 11b) are compared for different extraction conditions. Spectra are recorded with the same electron gun setting. The peak narrows when going from 1 mm slit (slit 1) to 0.2 mm slit (slit 2) for extraction conditions labelled "hh" ($U_{H4} = U_{H5}$ = 18 V and B = 7.3 mT). The peak further narrows when U_{H4} is lowered (U_{H4} = 7 V). Extraction conditions for U_{H4} = 7 V, U_{H5} = 18 V and B = 5.5 mT are labelled "ll". One spectrum is also shown for conditions labelled "lh" (U_{H4} = 7 V, U_{H5} = 18 V and B = 7.3 mT), showing the small influence of magnetic field on the peak shape. Extraction with U_{H4} = 7 V exhibited the best performances for lower magnetic fields.

Values of the relative transmission for the 14 eV peak, as determined for H^- and D^- for the extraction conditions U_{H4} = 7 V, U_{H5} = 18 V and B = 5.5 mT, and for different slits, are summarized in Table 2. A higher relative peak height was obtained for the 1 mm × 10 mm slit at h_1 = 3.8 mm (slit 4) than at h_1 = 3.5 mm (slit 3). This confirmed the model check with the CPO program that suggested increasing h_1 from 3.5 to 3.8 mm. There is almost no difference in transmission for two slit lengths (10 and 20 mm), confirming that there is strong focusing in the XY plane for these conditions with both lower U_{H4} and lower magnetic field. The trans-

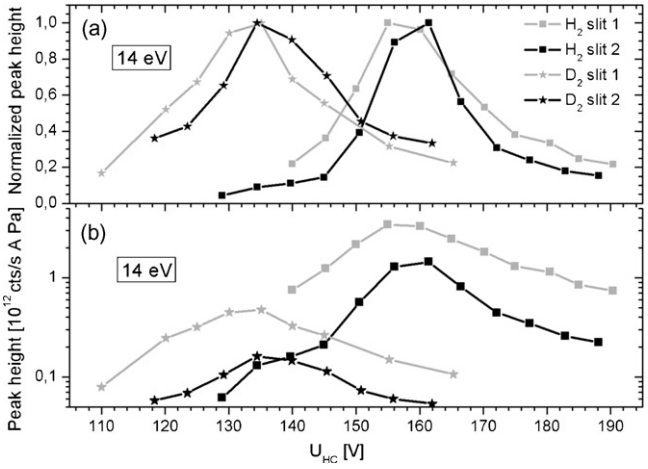

Fig. 10. (a) Normalized (linear scale) and (b) relative 14 eV peak height (logarithmic scale) versus U_{HC} are shown, for different widths of the S1 slit. Slit 1 stands for the slit 1 mm × 20 mm (height × width) and slit 2 for 0.2 mm × 20 mm both at h_1 = 3.5 mm. Other extraction conditions are B = 7.3 mT, $U_{H4} = U_{H5}$ = 18 V. Data for H^- are represented by squares and for D^- by stars.

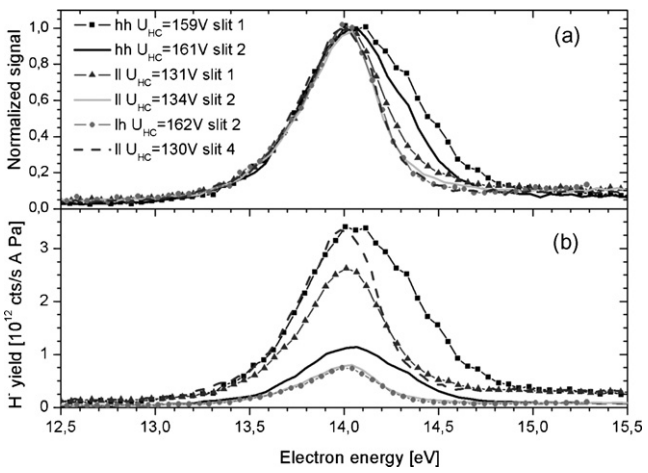

Fig. 11. The influence of different extraction conditions on the 14 eV peak shape (a) and its relative intensity (b). Values of U_{H4}, U_{H5} and B are as follows: "hh", $U_{H4} = U_{H5}$ = 18 V and B = 7.3 mT; "ll", U_{H4} = 7 V, U_{H5} = 18 V and B = 5.5 mT; "lh", U_{H4} = 7 V, U_{H5} = 18 V and B = 7.3 mT. Voltage on U_{HC} and slits S1 are marked on the graph.

Table 1
Summarized data for mass selectivity obtained from the normalized 14 eV peak height as a function of U_{HC} for both hydrogen isotopes for different extraction conditions

Slit #: height × width/h_1 [mm]: extraction conditions	H_{MAX} [V]	H_{FWHM} [V] ±10%	D_{MAX} [V]	D_{FWHM} [V] ±10%	Contribution		Mass selectivity
					H in D_{MAX}	D in H_{MAX}	
Slit 1:1 × 20/3.5: hh	155 ± 2	24	135 ± 2	28	0.16	0.32	1.54
Slit 2:0.2 × 20/3.5: hh	161 ± 2	16	134 ± 2	24	0.1	0.33	2.7
Slit 1: 1 × 20/3.5: ll	130 ± 2	21	105 ± 2	26	0.15	0.28	2.17
Slit 3: 1 × 10/3.5: ll	134 ± 2	20	107 ± 2	21	0.16	0.1	2.61
Slit 2: 0.2 × 20/3.5: ll	135 ± 2	21	107 ± 2	22	0.16	0.27	2.54
Slit 4: 1 × 10/3.8: ll	129 ± 2	18	102 ± 2	24	0.1	0.1	2.54

The H_{MAX} and D_{MAX} are U_{HC} voltages at which H^- and D^- exhibit the highest yield. FWHMs for respective mass selectivity peaks are also given. Relative contributions of H^- at D_{MAX} and D^- at H_{MAX} and mass selectivity defined as $4\,(H_{MAX} - D_{MAX})/(H_{FWHM} + D_{FWHM})$ are given in the last columns.

mission on the other hand decreases when slit 1 is replaced by the narrower slit 2, 3.2 times for H^- and 2.4 times for D^-. This decrease of the relative transmission is more pronounced for "ll" than for "hh" conditions, indicating weaker trajectory compression in the former case. On the other hand the relative transmission obtained with the slit 4 under "ll" conditions is almost equal to that for slit 1 under "hh" conditions (Fig. 11b).

Mass selectivity was determined experimentally for different S1 slits for the extraction conditions $B = 5.5$ mT, $U_{H4} = 7$ V and $U_{H5} = 18$ V. Data were analysed as for the case of "hh" extraction conditions, shown in Fig. 10a. The main characteristic results of the analysis, together with those for higher extraction voltage, are summarized in Table 1. Mass selectivity peaks for both isotopes still have similar asymmetric shapes (Fig. 10a). The U_{HC} voltage for maximum yield (H_{MAX} and D_{MAX}) and the full width at half maximum (FWHM) of the mass selectivity peak for H^- and D^- (H_{FWHM} and D_{FWHM}) are given in Table 1. The contributions of H^- at D_{MAX} and D^- at H_{MAX} and the parameter calculated as $4(H_{MAX} - D_{MAX})/(H_{FWHM} + D_{FWHM})$ are also shown. This parameter allows quantification of the quality of mass selectivity under specific extraction conditions.

The D^- transmission function for slit 3 (1 mm × 10 mm) decreases faster on the right side of the mass selectivity peak than for slit 1 (1 mm × 20 mm) and accordingly has a smaller FWHM. This indicates that the ions with higher energy that are badly focused in both planes do not pass through the shorter slit. In the case of slit 2 (0.2 mm × 20 mm) the D_{FWHM} is narrower than that of slit 1, but this is not a case for H_{FWHM}. In the case of slit 4 the mass selectivity is comparable to that of the slit 3, but its relative transmission (Fig. 11b and Table 1) is significantly higher under "ll" extraction conditions. These results lead to the conclusion that the focusing for the low extraction conditions is not as good as those for the higher extraction. Nevertheless, the relative transmission and mass selectivity are comparable to those for higher extraction conditions with slit 4. This analysis has shown that ion transmission is very sensitive to small change of position of the slit S1 (h_1).

The system was also analysed for various U_{H5} and various magnetic fields for some of these slits, with the result that the properties were not found to be as good as for the conditions presented above. For one test, S2 slit was removed, leaving the detector open with its 5 mm × 15 mm aperture. The signal increased by a factor of two but the mass selectivity was very poor, confirming the assumption from the CPO3D simulation that the S2 plays an important role in separating the two isotopes.

4.3. Absolute extraction effectiveness

For the quantitative analysis of extraction characteristics we deconvoluted the measured H^- peaks originating from DEA. This was done by comparing the experimental ion yield spectrum with a calculated model function obtained as a convolution of the cross section, an energy distribution function of incident electrons and an ion extraction effectiveness function. In this way, properties of ion extraction can be studied, assuming that the cross section is known from the literature and that the electron distribution function is determined separately. We assume the ion extraction effectiveness to be a function of the initial ion energy in the following form: for $E_i < P_1$ detection effectiveness is constant, i.e. $F(E_i) = 1$, and for $E_i > P_1$ it decreases exponentially:

$$F(E_i) = \exp(-P_2(E_i - P_1)). \quad (3)$$

The parameter P_2 determines the rate of decrease of $F(E_i)$ and, together with the parameter P_1, it determines the full width at half maximum of the extraction characteristic. The absolute extraction effectiveness is defined as $C_f \times F(E_i)$, where C_f is a normalization constant obtained by comparing measured ion yield with the yield calculated from the absolute cross section and experimental parameters. The constant C_f reflects the ion extraction effectiveness and the ion detection efficiency of the channel electron multiplier. This analysis is illustrated in Fig. 12.

In Fig. 12a, the experimental 4 eV peak is shown compared to the model function obtained by convolution of cross section (CS) from [16] with the electron energy distribution function (Eq. (2)) calculated with $T_C = 1900$ K and an optimized ion extraction function (Eq. (3)). The model function is normalized to the experimental relative peak intensity. The best fit parameters of $F(E_i)$ are $P_1 = 0.08$ eV and $P_2 = 10\ \text{eV}^{-1}$. A target temperature $T_g = 300$ K is assumed and all contributing rotational states are properly taken into account in the CS convolution. The shape of the low energy side of the 4 eV DEA peak is predominantly dependent on the electron energy distribution, due to the fact that CS exhibits a vertical threshold and that the low-energy part ($E_i < P_1$) of extraction effectiveness is constant. On the other hand, the high-energy part of the peak, where higher

Table 2
The maximum relative peak height (relative transmission) for different slits S1, for H^- and D^- ions

Slit #: height × width/h_1[mm]: extraction conditions	H^- relative 14 eV peak height [cts/s A Pa]	D^- relative 14 eV peak height [cts/s A Pa]
Slit 1: 1 × 20/3.5: hh	$3.4 \times 10^{12} \pm 5\%$	$4.7 \times 10^{11} \pm 7\%$
Slit 2: 0.2 × 20/3.8: hh	$1.4 \times 10^{12} \pm 8\%$	$1.6 \times 10^{11} \pm 13\%$
Slit 1:1 × 20/3.5: ll	$2.5 \times 10^{12} \pm 6\%$	$2.8 \times 10^{11} \pm 9\%$
Slit 3: 1 × 10/3.5: ll	$2.2 \times 10^{12} \pm 6\%$	$2.4 \times 10^{11} \pm 11\%$
Slit 2: 0.2 × 20/3.5: ll	$7.9 \times 10^{11} \pm 10\%$	$1.2 \times 10^{11} \pm 14\%$
Slit 4: 1 × 10/3.8: ll	$3.2 \times 10^{12} \pm 5\%$	$3.1 \times 10^{11} \pm 9\%$

Extraction conditions are marked with "hh" and "ll", where "hh" stands for $U_{H4} = U_{H5} = 18$ V, $B = 7.3$ mT, and "ll" for $U_{H4} = 7$ V, $U_{H5} = 18$ V, $B = 5.5$ mT.

energy ions are present (Eq. (1)), is strongly cut due to the decrease of ion extraction effectiveness with E_i (Eq. (3)).

The same model function that is shown in Fig. 12a is also shown in Fig. 12b but here together with DEA cross section [16] and two other convoluted functions, all in the absolute units of cross section. For better presentation, the theoretical cross section is convoluted with a very narrow, 12 meV wide, electron energy distribution, and rotational distribution at $T_g = 300$ K is taking into account. The second curve (dashed light grey line) is obtained by convolution of the theoretical CS by a Gaussian electron energy distribution function, with FWHM $\Delta E_{1/2} = 450$ meV that corresponds to the experimental resolution of Schulz and Asundi [17] (see [18] for discussion of the 4 eV peak shape). The third curve (dashed dark grey line) is obtained by CS convolution with a thermoionic electron energy distribution (Eq. (2), $T_C = 1900$ K, $\Delta E_{1/2} = 370$ meV) which corresponds to the present experimental conditions. Finally, the model function that also takes into account the extraction effectiveness, as determined for Fig. 12a, is shown as a solid grey line in Fig. 12b. The ratio of the peak value of convoluted cross section with the 12 meV Gaussian distribution to the peak value of convoluted cross section obtained for our detection system is 0.47. By comparing the experimental relative peak height from Fig. 12a with the absolute model function value from Fig. 12b, the absolute detection effectiveness can be determined by taking into account the basic definition of DEA CS. Thus, the absolute production yield of H^- ions in [cts/s] is calculated as:

$$Y_{\text{ion}} = N_{\text{el}} n_{\text{target}} l\sigma = \frac{I_{\text{el}}}{e}\frac{p}{kT} l\sigma, \tag{3}$$

where $N_{\text{el}} = I_{\text{el}}/e$ is the number of electrons crossing IR per second, $n_{\text{target}} = p/kT$ is the particle density of the target molecules in the interaction region, l is the length from which ions are extracted and σ is the cross section for DEA. Assuming the extraction length $l = 1$ cm and $T = 300$ K for the gas temperature, and using 2.32×10^{-25} m^2 (peak value of model function in Fig. 12b) for the 4 eV DEA CS under the present experimental conditions, the peak value of the absolute ion production yield normalized to the electron current and pressure is obtained. With these values the normalized yield is $S = Y_{\text{ion}}/I_{\text{el}}\ p = 3.5 \times 10^{12}$ cts/s A Pa. The ratio of the peak value of the measured normalized signal (0.28×10^{12} cts/s A Pa peak value of the model function in Fig. 12a) to the above normalized total ion yield gives the absolute detection effectiveness, $C_f = 0.081$. This value is the lower estimate of absolute detection effectiveness. The absolute value of the theoretical peak cross section from [16], when convoluted with 450 meV Gaussian distribution (shown in Fig. 12b), gives a peak value of 2.8×10^{-25} m^2 that is probably about 1.75 [16,18] to 2.3 [15] times higher than other experimental values found in the literature. Taking this into account we estimate that absolute effectiveness for detection of H^- by our system is 14–19%. A rough estimate of the absolute detection effectiveness made by comparing the signal intensity obtained in the present study with the experimental peak values of the 14 eV DEA measured by Rapp et al. [19], also gives a similar value of 20%.

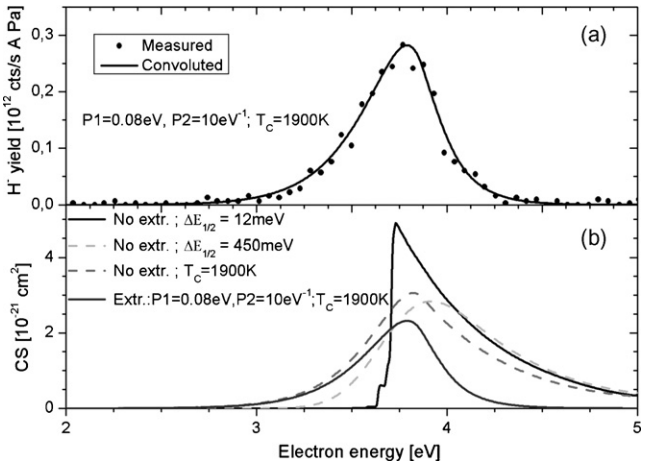

Fig. 12. Determination of the absolute detection effectiveness of the system. (a) The 4 eV peak recorded with low extraction conditions and with slit 4 (full circles) and the normalized convoluted spectrum (solid line). (b) The theoretical 4 eV DEA cross section convoluted with a Gaussian electron distribution function having FWHM $\Delta E_{1/2} = 12$ meV (solid black line) and $\Delta E_{1/2} = 450$ meV (dashed light grey line). The other two curves are the theoretical cross sections convoluted with electron distribution function as in (a) without (dashed dark grey line) and with (solid grey line) extraction selectivity.

4.4. Positive ions

The present extraction system was also tested by positive ion detection. To switch from negative to positive ion mode the direction of the magnetic field and the polarity of the extraction voltages have to be reversed. Also, the channel electron multiplier that serves as an ion detector has to be properly biased. For the study of positive ion detection a hydrogen atom source was used (HABS from Dr. Eberl MBE-Komponenten GmbH; http://www.mbe-components.com/) so that both hydrogen atoms and molecules were simultaneously present in the target gas. Hydrogen atoms are produced in this source by thermal dissociation in a radiatively and resistively heated tungsten capillary through which the hydrogen gas is introduced into the vacuum system. The capillary exit was placed at about 4 cm from the centre of the interaction region.

The threshold for hydrogen atom ionization by electron impact, $e + H \rightarrow H^+ + 2e$, is at 13.6 eV while the thresholds for ionization of the molecule, $e + H_2 \rightarrow H_2^+ + 2e$ or $e + H_2 \rightarrow H^+ + H + 2e$, are at 15.42 or 18.15 eV. The applied voltage to HC was scanned for extraction system analysis at an electron energy of 16.8 eV. This energy is above the threshold for atom and molecule ionization to the parent ions, therefore both H^+ and H_2^+ contribute to the ion yield. Regarding the ion mass, H^+ corresponds to H^-, and H_2^+ to D^- for the previous analysis with negative ions.

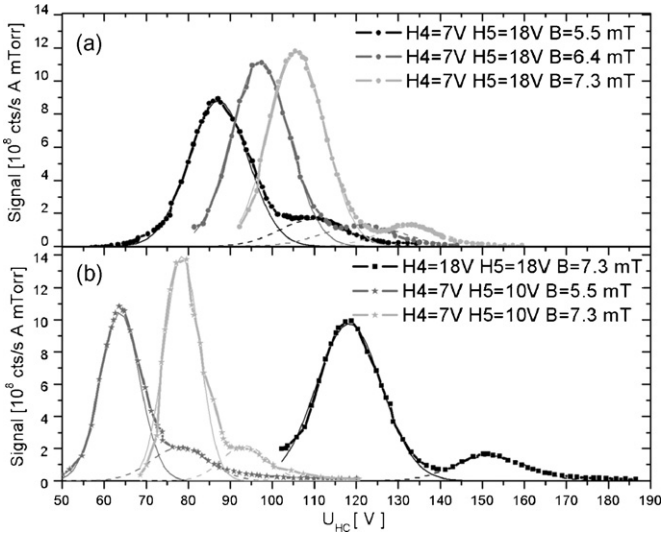

Fig. 13. Yield of positive ions versus U_{HC} at $E_e = 16.8$ eV, for the case of a partially dissociated target hydrogen gas. Electron energy is above thresholds for atom and molecule ionization into H^+ and H_2^+ respectively. Scans were performed under the extraction conditions labelled in the figure. In each spectrum two peaks are detected; the peak at the lower U_{HC} is due to H_2^+ (M/e = 2) and the peak at the higher U_{HC} is due to H^+. Multi-peak fits to the spectra using Gaussian peak shape are shown as solid lines.

Table 3
Extraction effectiveness for different ion masses and mass selectivity of the extraction system working in positive ion mode

Extraction conditions Slit 2: 0.2 × 20/3.5	H^+_{MAX} [V]	H^+_{FWHM} [V] ±2%	H^+ peak integral [10^7 cts/s A mTorr]	$H_2{}^+_{MAX}$ [V]	$H_2{}^+_{FWHM}$ [V] ± 2%	$H_2{}^+$ peak integral [10^8 cts/s A mTorr]	Mass selectivity
U_{H4} = 7 U_{H5} = 18 B = 5.5 mT	110 ± 2	15.6	2.9 ± 0.2	87 ± 1	14.4	1.53 ± 0.02	3.1
U_{H4} = 7 U_{H5} = 18 B = 6.4 mT	122 ± 2	18.7	3.1 ± 0.2	97 ± 1	13.8	1.93 ± 0.02	3.015
U_{H4} = 7 U_{H5} = 18 B = 7.3 mT	132 ± 2	17.6	2.3 ± 0.1	106 ± 1	13.1	1.97 ± 0.01	3.4
U_{H4} = 7 U_{H5} = 10 B = 5.5 mT	78 ± 2	13.5	3.5 ± 0.1	64 ± 1	9.4	1.23 ± 0.01	2.9
U_{H4} = 7 U_{H5} = 10 B = 7.3 mT	94 ± 2	11	3.0 ± 0.3	79 ± 1	8.3	1.45 ± 0.03	3.1
U_{H4} = 18 U_{H5} = 18 B = 7.3 mT	152 ± 2	16.9	3.3 ± 0.2	118 ± 1	15.6	1.9 ± 0.02	4.15

The contribution of individual ions to the total ion yield depends on the extraction conditions in a way similar to that discussed for negative ions. However, in contrast to the negative ion case, the nascent energy of positive ions is not electron energy dependent, since the excess energy of the process, $E = E_e - E_{Th}$ is mainly partitioned among the two exit electrons. The parent ion therefore has approximately the same kinetic energy as the target particle before ionization. The kinetic energy of H^+ created by electron–atom ionization is determined by the temperature of the surface where the atoms were created, while the energy of $H_2{}^+$ corresponds approximately to the thermal energy at the room temperature. Because the initial ion energy does not depend on electron energy the extraction analysis with positive ions is more straightforward than for the negative ion case. Here, information is obtained on both mass selectivity and detection effectiveness by a single ion yield scan over HC voltage at an appropriate electron energy. Some of the scans for different extraction conditions, with S1 slit 2 (0.2 mm × 20 mm at h_1 = 3.5 mm) are shown in Fig. 13. Temperature of the tungsten capillary and gas flow through the hydrogen atom source were the same for all measurements. Experimental ion yields are divided by the electron current and driving pressure at the high-pressure side of the tungsten capillary in the atom source to allow mutual intensity comparison. For the same electrode potentials as used for negative ions, but with reversed polarity (U_{H4} = −7 V and U_{H5} = −18 V), three spectra are shown in Fig. 13a for different magnetic fields. Two peaks can be distinguished in each spectrum: the first, at the lower U_{HC}, is due to the $H_2{}^+$ ions and the second to the H^+. By increasing the magnetic field the two peaks become more and more separated, but effectiveness for the two masses changes simultaneously, decreasing for H^+ and increasing for $H_2{}^+$. Similar phenomena are seen at U_{H5} = −10 V, where again at higher magnetic fields the peaks are more separated, Fig. 13b. In Fig. 13b, the spectrum with high U_{H4} is also shown.

By multi peak fitting of ion yield spectra, assuming Gaussian peak shape, the integral yield, widths and position of peaks are obtained for the contribution of a particular ion. The result of such an analysis of spectra obtained by different extraction conditions is shown in Table 3. The best conditions for good mass separation are at the higher extraction voltages, U_{H4} = −18 V, U_{H5} = −18 V and B = 7.3 mT. On the other hand the measured ion yield is less dependent on U_{H4} for both H^+ and $H_2{}^+$. This is the consequence of the thermal energy distribution of the created ions that are already effectively extracted with the lower extraction voltage. In contrast to the case of positive ions, the energy of negative ions is electron energy dependent, and ions with higher energy contribute more to the ion yield when U_{H4} is higher. Under low extraction conditions the peaks were best separated when U_{H4} = 7 V, U_{H5} = 18 V and B = 7.3 mT, at which values the highest ion yield for $H_2{}^+$ is also attained. The highest ion yield for H^+ ions was for U_{H4} = 7 V, U_{H5} = 10 V and B = 5.5 mT, but the mass separation was poorer.

In conclusion, the results of the study of the extraction performances of the present electrode system are very similar when carried out with positive and with negative ions.

5. Conclusions

We have developed and tested an effective extraction system for low energy hydrogen ions which combines basic extraction principles from electrostatic systems with a weak, superimposed magnetic field. Its main purpose is to be used for vibrational spectroscopy of hydrogen molecules. Both negative and positive ion modes have been analysed and are of interest for neutral hydrogen diagnostics. While the former is used to determine the vibrational population of neutral molecules, the latter is used for detecting neutral atoms in the target gas.

It is shown that proper consideration of the exact ion trajectories in a relatively weak magnetic field is indispensable for acquiring correct, quantitative data for low mass ions such as hydrogen. This is important for mass spectrometric studies involving light ions in similar experimental arrangements.

The new ion extraction system has been studied extensively under a variety of extraction conditions and optimal conditions have been determined. Optimal conditions of mass selectivity, transmission and DEA peak width were obtained with a 1 mm × 10 mm slit at h_1 = 3.8 mm and U_{H4} = 7 V, U_{H5} = 18 V and B = 5.5 mT. The absolute quantitative detection is estimated to be close to 20%.

The extraction system presented here has enabled new results to be obtained on dissociative electron attachment in H_2 and D_2 and also on vibrational distribution of molecules created by atom recombination on cold surfaces.

Acknowledgments

This work has been supported by the Research Agency of Republic of Slovenia (ARRS) project J1-6571 and program P1-0112. Work is also partially supported by the Project P2 of Association EURATOM-MHEST (Slovenian Fusion Association). Authors gratefully acknowledge the generosity of colleagues from the laboratory DIAM, Université Pierre et Marie Curie, Paris and CNRS, France for lending us a complete old electrostatic experimental set-up, which significantly facilitated our work.

References

[1] O. Ingólfsson, F. Weik, E. Illenberger, Int. J. Mass Spectrom. Ion Processes 155 (1996) 1.
[2] S.A. Rangwala, S.V.K. Kumar, E. Krishnakumar, N.J. Mason, J. Phys. B: At. Mol. Opt. Phys. 32 (1999) 3795.
[3] C. Bulliard, M. Allan, S. Grimme, Int. J. Mass Spectrom. 205 (2001) 43.
[4] P. Cicman, M. Francis, J.D. Skalný, T.D. Märk, Int. J. Mass Spectrom. 223–224 (2003) 271.
[5] D. Popović, I. Čadež, M. Landau, F. Pichou, C. Schermann, R.I. Hall, Meas. Sci. Technol. 1 (1990) 1041.
[6] C. Schermann, F. Pichou, M. Landau, I. Čadež, R.I. Hall, J. Chem. Phys. 101 (1994) 8152.
[7] I. Čadež, R.I. Hall, M. Landau, F. Pichou, M. Winter, C. Schermann, Acta. Chim. Slov. 51 (2004) 11.
[8] I. Čadež, S. Markelj, Z. Rupnik, S. Brezinsek, 33rd European Physical Society Conference on Plasma Physics, Roma, June 19–23, 2006. Contributed Papers, (Europhysics conference abstracts, vol. 30I). [Mulhouse Cedex]: European Physical Society, 2006 P4_175.

[9] I. Čadež, S. Markelj, Z. Rupnik, P. Pelicon, in: International Conference Nuclear Energy for New Europe, Portorož, Slovenia, 2006. Proceedings. Ljubljana, Nuclear Society of Slovenia, 2006, 507.1.
[10] S. Cvejanović, F.H. Read, J. Phys.B: At. Mol. Phys. 7 (1974) 1180.
[11] P. Lablanquie, S. Sheinerman, F. Penent, R.I. Hall, M. Ahmad, T. Aoto, Y. Hikosaka, K. Ito, J. Phys.B: At. Mol. Opt. Phys. 35 (2002) 3265.
[12] S. Markelj, Z. Rupnik, I. Čadež, in: 27th International Conference on Phenomena in Ionised Gases, Eindhoven, July 17–22, 2005, The Netherlands. *Proceedings*. Faculty of Applied Physics, Eindhoven, paper 08-237.
[13] L.A. Baranova, S.Ya. Yavor, F.H. Read, Rev. Sci. Instrum. 67 (1996) 756.
[14] P.W. Hawkes, E. Kasper, Principles of Electron Optics, vol. 2, Academic Press, 1989.
[15] I. Čadež, Z. Rupnik, S. Markelj, in: 27th International Conference on Phenomena in Ionised Gases, Eindhoven, July 17–22, 2005, The Netherlands. *Proceedings*. Eindhoven, Faculty of Applied Physics, paper 02-236.
[16] J. Horáček, M. Čižek, K. Houfek, P. Kolorenč, W. Domcke, Phys. Rev. A 70 (2004) 052712 (and private communication with authors).
[17] G.J. Schulz, R.K. Asundi, Phys. Rev. 158 (1967) 25.
[18] H. Drexel, G. Senn, T. Fiegele, P. Scheier, A. Stamatovic, N.J. Mason, T.D. Märk, J. Phys. B: At. Mol. Opt. Phys. 34 (2001) 1415.
[19] D. Rapp, T.E. Sharp, D.D. Briglia, Phys. Rev. Lett. 14 (1965) 533.